Published in "The Journal of Physical Chemistry A 110(49): 13332 -13340, 2006"
which should be cited to refer to this work.

DFT Studies on the Magnetic Exchange Across the Cyanide Bridge

Mihail Atanasov,*,†,‡,§ Peter Comba,*,‡ and Claude A. Daul*,§

Institute of General and Inorganic Chemistry, Bulgarian Academy of Sciences, Acad. Georgi Bontchev Str. Bl.11, 1113 Sofia, Bulgaria, Universität Heidelberg, Anorganisch-Chemisches Institut, Im Neuenheimer Feld 270, D-69120 Heidelberg, Germany, and Département de Chimie, Departement für Chemie, Ch.du Musée 9, CH-1700 Fribourg, Switzerland

Exchange coupling across the cyanide bridge in a series of novel cyanometalate complexes with $Cu^{II}-NC-M^{III}$ (M = Cr and low-spin Mn,Fe) fragments has been studied using the broken-symmetry DFT approach and an empirical model, which allows us to relate the exchange coupling constant with σ-, π-, and π*-type spin densities of the CN^- bridging ligand. Ferromagnetic exchange is found to be dominated by π-delocalization via the CN^- π pathway, whereas spin polarization with participation of σ orbitals (in examples, where the d_{z^2} orbital of M^{III} is empty) and π* orbitals of CN^- yields negative spin occupations in these orbitals, and reduces the $Cu^{II}-M^{III}$ exchange coupling constant. When the d_{z^2} orbital of M^{III} is singly occupied, an additional positive spin density appears in the σ(CN) orbital and leads to an increase of the ferromagnetic Cu−NC−M exchange constant. For low-spin $[M^{III}(CN)_6]^{3-}$ complexes, the d_{z^2} orbital occupancy results in high-spin metastable excited states, and this offers interesting aspects for applications in the area of molecular photomagnetism. The DFT values of the exchange coupling parameters resulting from different occupations of the t_{2g} orbitals of low-spin (t_{2g}^5) Fe^{III} are used to discuss the effect of spin−orbit coupling on the isotropic and anisotropic exchange coupling in linear Cu−NC−Fe pairs.

Introduction

The search for new molecular compounds with long-range magnetic order at room and higher temperatures is a main goal in the field of molecular magnetism.[1,2] One family of compounds with room-temperature magnetic behavior is that of the Prussian blue analogues. A breakthrough in this field has been the synthesis of a room-temperature magnet $V[Cr(CN)_6]_x \cdot nH_2O$ in 1995.[3] Surprisingly, the room-temperature magnetic behavior of this class of compounds is mainly due to antiferromagnetically coupled $t_{2g}^n-t_{2g}^{n'}$ ($n,n' < 6$) pairs of metal ions and a net magnetic moment imposed by mixed-valence, achieved by the control of stoichiometry.

Theoretical studies on the magnetic exchange via the CN bridge have been carried out on dinuclear model complexes using parametric models, such as the valence bond configuration interaction model,[4,5] and more sophisticate approaches based on Extended Hückel calculations,[6,7] the Kahn-Briat exchange coupling model,[8,9] the augmented spherical waves model,[10] Hartree−Fock,[11,12] and density functional theory.[12,13] A recent study on Prussion blue analogues discussed the importance of a systematic search for high-temperature magnetic complexes based on exchange coupling constants derived from broken-symmetry DFT calculations.[14] In these calculations, an efficient coupling mechanism via CN π orbitals has been shown to give rise to strong antiferromagnetic coupling, particularly pronounced in the case of $t_{2g}^4-t_{2g}^3$ ($Mn^{III}V^{II}$), $t_{2g}^3-t_{2g}^3$ ($Mo^{III}V^{II}$), $t_{2g}^3-t_{2g}^4$ ($Cr^{III}Mo^{II}$), $t_{2g}^2-t_{2g}^3$ ($V^{III}V^{II}$), and $t_{2g}^3-t_{2g}^3$ ($Cr^{III}V^{II}$) metal pairs. The symbiosis of π donation (for M^{III}) and π-back-donation (for M^{II}) plays an important role in all of these systems. Also, a potential ferromagnetic coupling of a reasonable magnitude in the case of the $t_{2g}^3-t_{2g}^6e_g^2$ $Mn^{IV}Ni^{II}$ pair has been demonstrated by these first-principles calculations.[14]

In broken-symmetry DFT studies, exchange coupling constants are extracted from the energies of the high-spin and the broken-spin single Slater determinants, from which a pure spin state can, in principle, be projected out. The analysis of the resulting exchange constant in terms of underlying orbital interactions is difficult if not impossible. However, an interesting correlation between exchange coupling constants from broken-symmetry DFT calculations and spin densities for the high-spin and low-spin Slater determinants have been demonstrated in dinuclear azido-bridged copper complexes[15] and recently been extended to cyanide-bridged Prussian-blue-type model compounds.[14] Qualitative discussions that relate the spin density with the exchange coupling constant,[16] covering cases of weak to moderate exchange coupling, deserve further quantitative analysis. It is therefore tempting to look for a more explicit connection between the exchange coupling constant in cyano-bridged complexes and the spin density on the cyanide bridging ligand.

It is well-known that current implementations of Kohn−Sham DFT cannot account for orbital degeneracy in a proper way.[17,18] Thus, although calculations of the exchange coupling between transition-metal ions with nondegenerate ground states (such as $Ni^{II}-NC-Cr^{III}$) can be done routinely, this is not the case for ions such as Mn^{III} and Fe^{III} in their low-spin ($^3T_1$ and $^2T_2$) orbitally degenerate ground states. An average-of-configurations Kohn−Sham formalism with evenly occupied d orbitals (non-integer occupations) have been applied within the constraint of high symmetry.[19−23] Alternatively, different exchange coupling constants for different electronic configurations from the degenerate $^3T_1$ or $^2T_2$ ground states have been shown to lead to orbitally dependent (non-Heisenberg) exchange coupling.[24−26]

* Corresponding authors. Address: Universität Heidelberg. Fax (+49) 6221-546617. E-mail: peter.comba@aci.uni-heidelberg.de; mihail.atanasov@aci.uni-heidelberg.de; claude.daul@unifr.ch.

† Bulgarian Academy of Sciences.

‡ Universität Heidelberg.

§ Département de Chimie.

Therefore, we wanted to explore whether reported single determinant BS-DFT values for the exchange coupling constant in cyanide-bridged transition metals with degenerate T_1 and T_2 ground states[14] are physically relevant.

Recently, we have prepared and characterized a series of oligonuclear cyanometalates.[27] They include Cu^{II} coordinated to four sp^3-nitrogen atoms from a tetraazamacrocyclic ligand and $M^{III}(CN)_6^{3-}$ ($M^{III} = Cr^{III}$ (d^3) and low-spin $Mn^{III}(d^4)$ and $Fe^{III}(d^5)$ complexes). Cu^{II} is a Jahn−Teller-active metal ion and tends to afford short and strong equatorial bonds, and long and weak bonds to the terminal N atoms of the bridging cyanide ligands. Depending on the system, these weak bonds can span a wide range of Cu−N distances, which vary between 2.25 and 2.57 Å. As expected for the long Cu−(NC)M bond distances and the orthogonality of the magnetic orbitals [$\sigma(d_{x^2-y^2})$for Cu(II), π (d_{xz}, d_{yz}, and d_{xy}) for the $t_{2g}{}^nM^{III}$ ions ($n = 3$ (Cr^{III}), $n = 4$ (Mn^{III}), $n = 5$ (Fe^{III})], the magnetic interaction in these systems are weak and ferromagnetic.

Here, we study the dependence of the exchange coupling in complexes with Cu^{II}−NC−M^{III} bridges on the electronic configuration of the low-spin $[M(CN)_6]^{3-}$ (M = Cr, low-spin Mn and low-spin Fe). An analysis of the ferromagnetic exchange coupling constants in terms of the spin densities[28] on the cyanide bridge allows us to deduce for the first time the effect of M−CN σ and π donation, and π* back-donation, and to study in detail the relative importance of spin delocalization and spin polarization for the magnetic exchange across the cyanide bridge. The dependence of the exchange coupling constant on the electronic configuration of the degenerate ground state of $Mn^{III}(t_{2g}{}^4)$ and $Fe^{III}(t_{2g}{}^5)$ is also described. Orbital degeneracy in these ground states may be lifted by Jahn−Teller distortions, however. DFT values of the exchange coupling parameters from different occupantions of the t_{2g} orbitals of low-spin ($t_{2g}{}^5$) Fe^{III} as well as spin−orbit coupling are used to characterize the isotropic and anisotropic exchange coupling constant in the linear Cu−NC−Fe exchange pair.

Theoretical Background and Computational Details

Exchange Coupling Constants from DFT Calculations. The exchange coupling constants (J_{BS}) have been calculated using DFT and the broken-symmetry approach (BS-DFT).[29,30] For isotropic exchange coupling with a Heisenberg Hamiltonian (eq 1) J_{BS} is given by eq 2, which is valid under the assumption of a weak overlap (S_{12}) between the magnetic orbitals ($S_{12}{}^2 \ll 1$).

$$H_{ex} = -J\cdot\mathbf{S_1}\cdot\mathbf{S_2} \tag{1}$$

$$J_{BS} = (E_{BS} - E_{HS})/(2\cdot S_1\cdot S_2) \tag{2}$$

The term $E_{BS} - E_{HS}$ represents the energy difference between the total energies of two spin-unrestricted DFT calculations; one for the high-spin $M_s = S_1 + S_2$ state, which affords the energy E_{HS}, and the other for an $M_s = |S_1 - S_2|$ determinant with energy E_{BS}. The latter is obtained from a spin-polarized DFT calculation by breaking the spin symmetry, that is, by imposing spin polarization of different sign on the two magnetic centers. It has been shown that this method allows us to account for a large part of the electronic correlation and it is generally applied in DFT calculations.[31] However, if antiparallel spin alignment is favored, then values of J_{BS} exceed the experimental values typically by a factor of 2. The origin of this discrepancy and possibilities for corrections have been discussed, and this still is subject to controversy.[32−34]

Here, DFT values of exchange coupling constants are calculated with eqs 1 and 2 and a PW91 functional. Our aim is to understand the factors that affect the exchange coupling and its anisotropy, rather than to obtain accurate values of the exchange coupling constant. However, the effect of the functional, in particular the changes that emerge when changing from the pure (PW91) to a hybrid (B3LYP) functional and the effect of the different basis sets are addressed.

Correlation between Spin Density and Magnetic Exchange. The first attempt to correlate magnetic exchange with spin densities on interacting atoms was based on a phenomenological Hamiltonian for the interaction of two subsystems (organic radicals) A and B[35]

$$H^{AB} = -\sum_{i,j} J_{ij}^{AB}\, \mathbf{S}_i^A\cdot\mathbf{S}_j^B \tag{3}$$

where $\mathbf{S}_i^A$ and $\mathbf{S}_j^B$ are spins $i(j)$ of $s = {}^1/_2$ on A the radicals (B) and

$$J_{ij} = [ij|ij] - 4\,\frac{\langle i|h|j\rangle^2}{U} \tag{4}$$

In eq 4 $[ij|ij]$ is the two-electron exchange coupling constant, $\langle i|h|j\rangle$ is the transfer (hoping) constant, and U is the on-site Coulomb repulsion parameter. The two terms in eq 4 are of different sign. The first term is positive and favors ferromagnetic spin alignment (potential exchange). The second term is negative and tends to lead to an antiferromagnetic coupling. It reflects delocalization of the magnetic electrons connected with gain of kinetic energy (kinetic exchange). Equation 3 can be written in the form[35]

$$H^{AB} = -J_{AB}\,\mathbf{S^A}\cdot\mathbf{S^B} = -\mathbf{S^A}\cdot\mathbf{S^B}\sum_{ij} J_{ij}^{AB}\,\rho_i^A\,\rho_j^B \tag{5}$$

where $\mathbf{S^A}$ and $\mathbf{S^B}$ are the total spin operators for A and B and ρ_i^A and ρ_j^B are the corresponding spin densities. Therefore, the exchange coupling constant between two extended magnetic units A and B is approximated by a sum over exchange parameters, which belong to interactions between their constituent units, J_{ij}^{AB}, and are weighted by the product of spin densities:

$$J_{AB} = \sum_{ij} J_{ij}^{AB}\,\rho_i^A\,\rho_j^B \tag{6}$$

Equation 6 has been applied to organic radicals with spins i and j, which are in close contact and are stacked on top of each other such that $J_{ij}^{AB} < 0$ (i.e., the second term in eq 4 dominates). It follows that coupling between A and B is antiferromagnetic when both ρ_i^A and ρ_i^B are positive, and it is negative if ρ_i^A and ρ_i^B are of different sign. It has been pointed out[36,37] that eqs 5 and 6 are not based on a rigorous theory but are purely phenomenological. It has been shown, however, by valence bond calculations, that they can be applied in highly symmetric situations in which one interaction term (within the sum of eq 6) dominates over the other terms.

If we regard the Cu−M^{III} exchange pair as composed of two units $[Cu(NH_2CH_3)_4]^{2+}$ (Cu) and the $[M(CN)_6]^{3-}$ (NCM) subunits, then we can present the exchange Hamiltonian in an alternative form, eq 7, where J_{CuM} is the exchange coupling constant between the Cu and M magnetic centers, and J_{Cu-NCM} is the exchange coupling constant between the $[Cu(NH_2CH_3)_4]^{2+}$ (Cu) and $[M(CN)_6]^{3-}$ (NCM) units as a whole.

$$H_{exc} = -J_{CuM}\cdot\mathbf{S}_{Cu}\mathbf{S}_{M} = -J_{Cu-NCM}\mathbf{S}_{Cu}\mathbf{S}_{NCM} \quad (7)$$

Furthermore, with the concept of local spins[38−40] we can represent the total spin $\mathbf{S}_{NCM}$ as a sum of $\mathbf{s}_N$, $\mathbf{s}_C$, and $\mathbf{s}_M$ local spins, that is

$$\mathbf{S}_{NCM} = \mathbf{s}_N + \mathbf{s}_C + \mathbf{s}_M + ... \quad (8)$$

and the spin density on NCM, ρ_{NCM}, as the sum of ρ_N, ρ_C, and ρ_M. In analogy to eq 6

$$J_{Cu-NCM} = J_{Cu-N}\,\rho_N + J_{Cu-C}\,\rho_C + J_{Cu-M}\,\rho_M \approx J_{Cu-N}\,\rho_N \quad (9)$$

where only one term, that due to N with the closest contact to Cu, is considered. J_{Cu-N} is the spin coupling energy due to to unit spin density on N. It is worth noting that, because of the vanishing overlap, the value of J_{Cu-N} is given by the first term of eq 4 and is positive. Spin densities of the same sign on Cu and N lead to ferromagnetic coupling, while spin densities of different sign lead to antiferromagnetic coupling. We will compare exchange coupling constants, obtained from a BS DFT approach with spin densities ρ(N), deduced from spin-unrestricted DFT calculations on the $[M^{III}(CN)_2(NH_3)_4]^{1+}$ and $[M^{III}(CN)_6]^{3-}$ subunits. In a refined treatment, we have to consider spin populations on the σ and π orbitals $3a_1(\sigma)$ and $1e(\pi)$, and on the empty and (antibonding) 2e π^* orbital of CN^- (Figure 1), which we denote ρ_σ, ρ_π, and ρ_π^*, respectively (eq 10). These spin populations arise from spin delocalization and/or spin polarization induced on the nominally diamagnetic CN^- ligand, due to the overlap of its empty and doubly occupied orbitals with those of M^{III}, which carry the unpaired d electrons.

$$J_{Cu-NCM} \approx \rho_\sigma\cdot j_\sigma + \rho_\pi\cdot j_\pi + \rho_\pi^*\cdot j_\pi^* \quad (10)$$

The values of j_σ, j_π, and j_π^* are approximated with BS-DFT calculations and a model complex, which consists of the Cu^{II} amine complex and a CN radical with a single electron placed on the $3a_1(\sigma)$, $1e(\pi)$, and 2e (π^*) orbitals.

Computational Details. Density functional calculations have been carried out using the Amsterdam density functional (ADF) program[41−46] with the local density (LDA) and generalized gradient approximation (GGA). The LDA was applied with the Vosko−Wilk−Nusair (VWN)[47] local density potential and the GGA was applied by using Perdew-Wang91 (PW91)[48,49] exchange-correlation functional. Large Slater-type orbital (STO) (triple-ζ) basis sets with one polarization function (p-type for hydrogen, d-type for C and N) and the frozen core approximation have been used up to 3p for metals and up to 1s for carbon and nitrogen.

All of our attempts to get an SCF convergence of a $\{Cu(NH_2CH_3)_4NCCr(CN)_5\}^{1-}$ complex while keeping Cu^{II} and Cr^{III} in their nominal d^9 and d^3 configurations failed, probably due to some deficiencies of the basis sets of Cu [15] and/or of the used functional. As expected, orbitals of Cu^{II} are lower in energy than those of Cr^{III}. Because of the highly negative (−3) charge on $[Cr(CN)_6]^{3-}$, a flow of electron charge localized mostly on equatorial CN ligands toward the 3d orbitals of Cu^{II} took place, resulting in a reduction of Cu from a nominal (II) to a (I) valence state. Although this is a well-known fact from Cu-cyanide chemistry with disproportionation of $Cu(CN)_2$ into CuCN and $(CN)_2$, it is an artifact for the rather weak Cu −NC interaction. To circumvent this difficulty, we have chosen a Cu^{II}−NC−Cr^{III} model complex with a geometry obtained from a DFT geometry optimization (Figure 2) and have taken this geometry without changes for the M^{III} = Mn and Fe complexes.

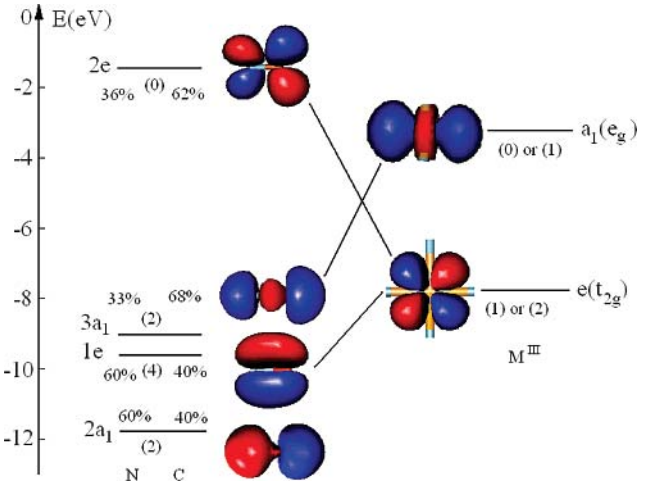

Figure 1. Orbitals on the CN^- bridges coupled with the e_g and t_{2g} orbitals of the transition-metal ions M^{III}.

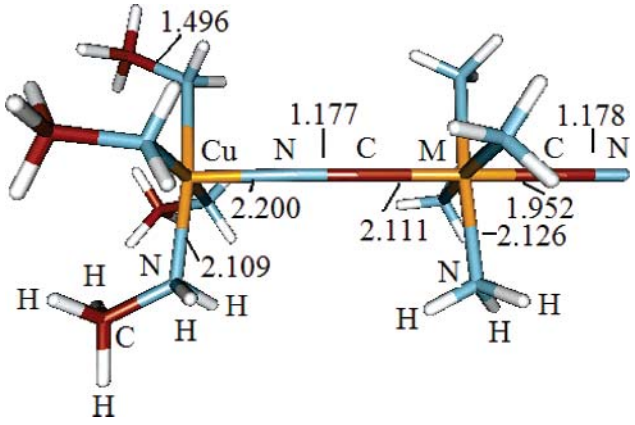

Figure 2. Dinuclear DFT (PW91) geometry-optimized Cu^{II}−NC−Cr^{III} model complex adopted for the calculation of the BS-DFT exchange coupling constants of Cu^{II}−NC−M^{III} (M^{III} = Cr, Fe, Mn).[16]

To check the inherent approximations due to this simplified model, calculations with ORCA[50] and the TZVP basis sets or SVP basis sets and a B3LYP functional have been done. With the program ORCA and a charge-compensating continuum model (COSMO), exchange coupling constants and spin densities for the Cu^{II}−NC−Cr^{III} model complexes and $[Cr(CN)_6]^{3-}$ have been compared and showed no significant effect on replacement of terminal CN by NH_3, and no essential dependence on the basis set (TZVP vs SVP). However, with a PW91 geometry-optimized Cu^{II}−NC−Cr^{III} model complex, J_{BS} values are found to be in better agreement with experiment than those obtained with the B3LYP functional.

To explore the effect of the non-CN ligand in the *trans*-$[M^{III}(NH_3)_4(CN)_2]^+$ model complexes on the magnetic exchange, and to get spin densities on the CN-bridging ligand, spin-unrestricted DFT calculations on *trans*-$[M^{III}(NH_3)_4(CN)_2]^+$ and $[M^{III}(CN)_6]^{3-}$ (M^{III} = Cr, Mn, Fe) model complexes have been caried out, both on the bare ions and in the latter case of charge-compensated species. Use of the conductor-like screening model (COSMO),[51] as implemented in ADF,[52] has been made. We adopted the dielectric constant of water (ϵ = 78.4) with the solvent radii (in Å) of 1.00 (M^{III} = Cr, Mn, Fe), 2.10 (C), and 1.40 (N).

Results and Discussion

Dependence of the $Cu^{II}\cdots Cr^{III}$ Exchange Coupling Constant on the Cu−NC−Cr Geometry. Values of the Cu^{II}−Cr^{III}

TABLE 1: Dependence of the Exchange Coupling Constant (in cm^{-1}) from a Broken-Symmetry DFT Calculation (J_{BS}) on the Cu−NCCr Distance *R* (in Å)

R	2.10	2.20	2.30	2.40	exptl[a]
J_{BS}	8.9	6.5	4.4	3.6	6.8

[a] Experimental distance $R = 2.247$ Å; *R* distance for the PW91 optimized geometry, $R = 2.20$ Å.

exchange constant J_{BS} in dependence of the Cu−N distance, *R*, for a linear Cu−C−N−Cr bridge are listed in Table 1. J_{BS} is positive and small, reflecting a weak Cu−Cr ferromagnetic coupling. As expected, J_{BS} decreases with increasing *R*. We have explicitly checked the effect of the adopted functional, the basis set, and the replacement of terminal CN^- by NH_3 ligands (see the Supporting Information). A value of J_{BS} [$R = 2.2$ Å, 6.5 cm^{-1} (PW91, ADF), 6.8 cm^{-1} (PW91, ORCA)] in better agreement with experiment ($J = 6.8$ cm^{-1})[27] was obtained when using a PW91 functional instead of the B3LYP functional [$J = 3.8$ cm^{-1} (ORCA), TZVP basis in all calculations]. The change from a triple to double-ζ basis (6.8 vs 5.4 cm^{-1}) does not affect J_{BS} significantly. In line with spin density analysis (see below), small changes of the value of J_{BS} were found when replacing NH_3 by CN (6.8 vs 7.3 cm^{-1}, PW91-functional, TZVP basis, ORCA).

Spin Densities and Exchange Coupling in Weakly Coupled Cu−NC−M^{III} (M^{III} = Cr^{III}, Mn^{III}, Fe^{III}) Exchange Pairs. J_{BS} values for the Cu−NC−M^{III} pairs (J_{BS}) are listed in Table 2. Different electronic states have been considered in the case of the Mn^{III} and Fe^{III} complexes. These include the $^3A_2$ ($b_2^1e^2$) and ^3E ($b_2^1e^3$) electronic states of Mn^{III}, which result from the low-spin t_{2g}^4 configuration of the parent octahedral $^3T_{1g}$ term, and the $^2B_2$ ($b_2^1e^4$) and ^2E ($b_2^2e^3$) electronic states split out from the $^2T_{2g}$ ground state of low-spin octahedral Fe^{III}. In addition, results for the high-spin states, $^5A_1$ ($b_2^1e^2b_1^1$) and $^5B_1$ ($b_2^1e^2a_1^1$) for Mn^{III} and $^6A_1$ ($b_2^1e^2b_1^1a_1^1$) for Fe^{III}, have been included in Table 2. To facilitate comparison between the values of J_{BS} for the Cu^{II}−M^{III} pairs with different electronic and spin states on M^{III}, we list in Table 2 the product $n_a \cdot n_b \cdot J_{BS}$. It is the quantity that sums up from contributions ($j_{\mu\nu}$) over different magnetic orbitals, and thus is particularly easy to interpret. Thus, for Mn^{III} $^5B_2$ ($b_2^1e^2b_1^1$), for example, we have

$$n_a \cdot n_b\, J_{BS}(\mathrm{Cu-Mn}) = j_{x^2-x^2,xy} + j_{x^2-y^2,xz} + j_{x^2-y^2,yz} + j_{x^2-y^2,x^2-y^2} \quad (11)$$

As immediately follows from an inspection of the data in Table 2, the exchange is particularly efficient for M^{III} with singly occupied e and a_1 orbitals possessing π and σ symmetries with respect to the bridging CN-ligand. The exchange becomes weaker when lowering the number of such singly occupied orbitals, for example, in the case of Mn^{III}-^3E ($b_2^1e^3$) compared to Mn^{III}-$^3A_2$(b^2e^2), and nearly vanishes for the Fe^{III} $^2B_2$ ($b_2^1e^4$) state with an unpaired electron in the d_{xy} orbital of δ symmetry with respect to CN.

Atomic spin densities as deduced by Mulliken population analysis are listed in Table 3.

Spin densities do not change significantly if Löwdin charges are used instead (see the Supporting Information). Although the total spin density on the bridging N [ρ(N)] is calculated to be comparatively large and positive in all cases (except for Fe^{III}-$^2B_2$ [$b_2^1e^4$]) it is negative on C [ρ(C)] in those cases, where the a_1 (d_{z^2})-orbital on M^{III} is empty. However, ρ(C) becomes zero or even positive for Mn^{III}-$^5B_1$ ($b_2^1e^2a_1^1$) and Fe^{III}-$^6A_1$ ($b_2^1e^2b_1^1a_1^1$) with a singly occupied a_1 (d_{z^2}) orbital. An interesting correlation between $n_a \cdot n_b J_{BS}$ and ρ(N) was established (Figure 3), consistent with eq 9. At the same time, we notice significant deviations from the correlation line (Figure 3), which are positive in the case of $^6A_1$(Fe) and negative in the case of $^5A_1$(Mn) (see underlined entries in Figure 3). These are also the two cases with a singly occupied or empty d_{z^2} orbital, respectively.

TABLE 2: Exchange Coupling Energies from Broken-Symmetry DFT Calculations of a Series of $[Cu(NH_2CH_3)_4-NC-M^{III}CN(NH_3)_4]^{1-}$ Exchange Coupled Model Complexes (M^{III} = Cr^{III}, Mn^{III}, Fe^{III}) with Various Electronic States at the *trans*-$M^{III}(NC)_2(NH_3)_4$ Fragment with Spin Populations on CN from Spin-Unrestricted DFT Calculations on the Latter Fragments[a]

Cu^{II}−M^{III} pair (M^{III} electronic configuration)	J_{BS}	$n_a \cdot n_b \cdot J_{BS}$	ρ(N)	ρ(C)
Cu^{II}−NC−Cr^{III}				
$^4B_1(b_2^1e^2)$	6.5	19.5	0.114	−0.135
Cu^{II}−NC−Mn^{III}				
$^3A_2(b_2^2e^2)$	10.4	20.8	0.114	−0.107
^3E ($b_2^1e^3$)	5.2	10.4	0.063	−0.074
$^5A_1(b_2^1e^2b_1^1)$	3.0	12.0	0.098	−0.146
$^5B_1(b_2^1e^2a_1^1)$	6.2	24.8	0.114	0.000
Cu^{II}−NC−Fe^{III}				
$^2E(b_2^2e^3)$	16.6	16.6	0.078	−0.045
$^2B_2(b_2^1e^4)$	−1.0	−1.0	−0.009	−0.028
$^6A_1(b_2^1e^2b_1^1a_1^1)$	8.7	43.5	0.151	0.059

[a] C_{4v} point group symmetry notations for the electronic terms of Cr^{III}, Mn^{III}, and Fe^{III} have been used.

We now focus on the spin density on the bridging CN ligand and concentrate on the corresponding contributions from σ- and π-type orbitals. In Table 3 we report spin populations for these orbitals on C and N, for both *trans*-$[M(NH_3)_4(CN)_2]^+$ and $[M(CN)_6]^{3-}$ (M = Cr^{III}, Mn^{III}, and Fe^{III}). We first focus on the former complex. As discussed in ref 16, spin densities on ligands, induced by their bonding to a paramagnetic transition metal ion are due to two possible mechanisms: spin delocalization and spin polarization. In the former, spin density, which initially belongs to the metal ion, is redistributed to orbitals of the closed shell ligand that overlaps with the metal d orbitals. Taking, for example, one unpaired spin on the t_{2g} orbital, initially localized on M^{III}, this leads to the spin population in orbital μ on ligand A, ρ_μ(A), as given by eq 12

$$\varphi_{t_{2g}} = \sum c_{t_{2g},\mu}\chi_\mu$$

$$\rho_\mu(A) = \sum_\nu c_{t_{2g},\mu} \cdot c_{t_{2g},\nu} S_{\mu\nu} \quad (12)$$

The spin polarization mechanism is more subtle. It arises from the natural tendency of unpaired electrons on orthogonal orbitals to orient parallel in a given atom. If there is initially one electron pair on a ligand and a single electron of α spin on the metal ion, then partial formation of a pair of α spins concentrated on the metal ion and occupying orthogonal orbitals will necessarily generate a net β spin density on the ligand.

To illustrate the operation of the two mechanisms, we take (t_{2g}^3) Cr^{III}−CN as an example.

Transfer of β spins from the occupied 1e CN π orbital to the half-filled t_{2g}^3 shell creates positive spin density on this orbital, and transfer of α spin of Cr^{III} to the empty 2e(π^*) orbital creates also a positive spin density on this antibonding orbital (Figure 4a). The e_g orbitals of Cr^{III} are empty; therefore, transfer of α spins from the doubly occupied $3a_1$ to the e_g (d_{z^2})-type orbital of Cr^{III} creates β spin density on the CN ligand. This is favored over the transfer of β spins due to intra-atomic (Hund) exchange,

TABLE 3: Spin Densities on the CN Bridging Ligand that Originate from Spin Polarization and Spin Delocalization, Due to Open-Shell Paramagnetic Transition Metal Ions in *trans*-$[M(NH_3)_4(CN)_2]^+$ (A) and $[M(CN)_6]^{3-}$ (B) (M = Cr^{III}, Mn^{III} and Fe^{III}), and Their Decomposition into Contributions from the σ(CN), π(CN), and π^*(CN) Orbitals of Cyanide[a]

$Cu^{II}-M^{III}$ pair (M^{III} electronic configuration)	ρ_σ(C)	ρ_π(C)	ρ_σ(N)	ρ_π(N)	ρ_σ	ρ_π	ρ_{π^*}
$Cu^{II}-NC-Cr^{III}$							
$^4B_1(b_2^1e^2)$							
A	−0.075	−0.060	0.001	0.113	−0.092	0.213	−0.159
B	−0.076	−0.060	0.004	0.121	−0.093	0.226	−0.165
$Cu^{II}-NC-Mn^{III}$							
$^3A_2(b_2^2e^2)$							
A	−0.059	−0.048	0.000	0.114	−0.072	0.209	−0.143
B	−0.058	−0.047	0.003	0.105	−0.071	0.193	−0.136
$^3E(b_2^1e^3)$							
A	−0.046	−0.028	−0.004	0.067	−0.056	0.122	−0.083
B	−0.044	−0.034	0.000	0.048	−0.055	0.094	−0.080
$^5A_1(b_2^1e^2b_1^1)$							
A	−0.091	−0.055	−0.009	0.107	−0.112	0.200	−0.148
B	−0.083	−0.059	0.001	0.102	−0.102	0.194	−0.151
$^5B_1(b_2^1e^2a_1^1)$							
A	0.031	−0.031	0.008	0.106	0.038	0.188	−0.112
B	0.087	−0.026	0.005	0.078	0.107	0.139	−0.087
$Cu^{II}-NC-Fe^{III}$							
$^2E(b_2^2e^3)$							
A	−0.028	−0.017	−0.001	0.079	−0.034	0.137	−0.074
B	−0.028	−0.022	0.001	0.048	−0.030	0.088	−0.062
$^2B_2(b_2^1e^4)$							
A	−0.024	−0.004	−0.007	−0.002	−0.030	−0.001	−0.005
B	−0.020	−0.007	−0.002	−0.005	−0.025	−0.004	−0.008
$^6A_1(b_2^1e^2b_1^1a_1^1)$							
A	0.069	−0.010	0.015	0.136	0.085	0.226	−0.100
B	0.118	−0.014	0.008	0.065	0.145	0.113	−0.062

[a] C_{4v} point group symmetry notations for the electronic terms of Cr^{III}, Mn^{III}, and Fe^{III} have been used.

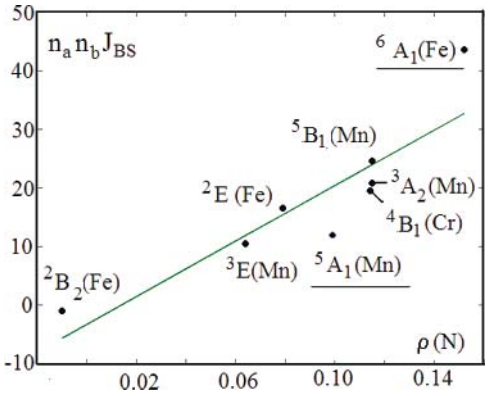

Figure 3. Correlation between the $Cu-NC-M^{III}$ (M^{III} = Cr^{III}, Mn^{III}, Fe^{III}) exchange energy $n_a n_b J_{BS}$ and the spin density on N.

which tends to stabilize parallel spins on Cr^{III}. Therefore, negative spin densities ρ_σ(C) (Table 3) can be understood, based on a spin polarization. In support of this interpretation, we find positive ρ_σ(C) values in cases with a singly occupied a_1 orbital on M^{III} (Figure 4b). The situation changes with π-type spin densities. Although ρ_π(N) is positive, in line with a spin delocalization mechanism, ρ_π(C) is negative. As follows from spin restricted calculations, there is no electron population on the carbon π-orbitals of the CN ligand in the ground state of the $Cr^{III}-CN$ complex. Therefore, the spin density found on the carbon π orbitals originates from the interplay between spin polarization and spin delocalization.

The spin densities in Table 3 are qualitatively in agreement with polarized neutron diffraction experiments of $Cs_2KCr(CN)_6$.[53,54] The computed spin densities also agree with spin-density distributions in $Cs_2K[Fe(CN)_6]$ and $Cs_2K[Mn(CN)_6]$ deduced from high-resolution magic angle spinning NMR spectra.[55] The comparison shows within the experimental and computational accuracy that spin densities are overestimated by DFT, typically by a factor between 2 and 10.

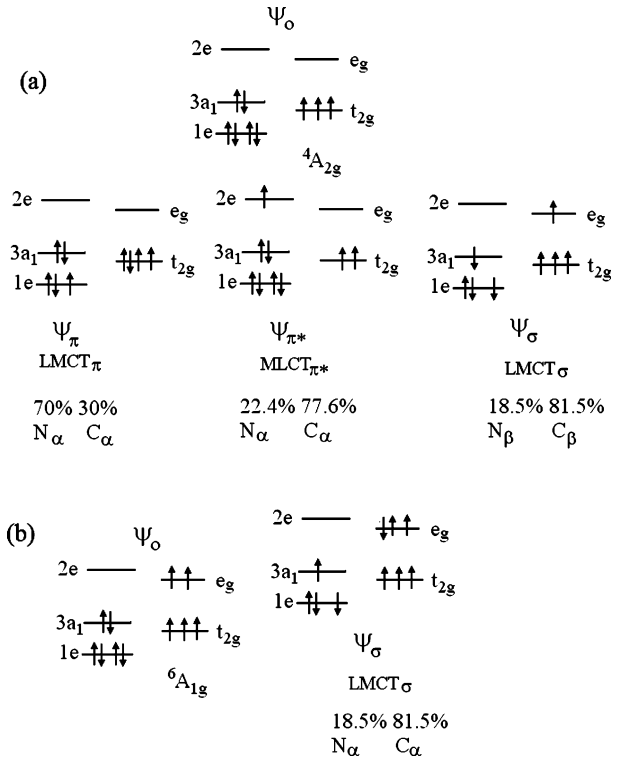

Figure 4. (a) Ground-state and charge-transfer configurations leading to spin delocalization of the Cr^{III} spins toward the CN bridge. (b) The high-spin excited state and the excited LMCT charge-transfer state, which lead to positive spin density on the $3a_1$ σ orbital of CN^- in the case of $[Fe(CN)_6]^{3-}$.

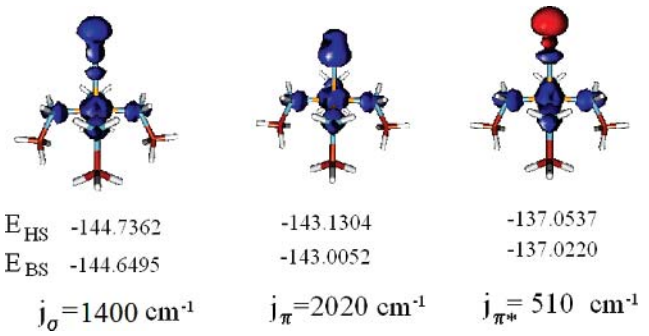

Figure 5. Spin densities for the $S = 1$ state, resulting from the coupling of the $s = {}^1/_2$ spin $[Cu(NH_2CH_3)_4]^{2+}$ with a $s = {}^1/_2$ CN radical with a single electron placed on the $\sigma(3a_1)$, $\pi(1e)$, and $\pi^*(2e)$ orbitals; exchange coupling constants extracted from the HS and BS DFT energies are also given.

If we confine to a model in which only $3a_1$, 1e, and 2e contribute to $\rho_\sigma(C)$, $\rho_\pi(C)$, $\rho_\sigma(N)$, and $\rho_\pi(N)$, spin densities ρ_σ, ρ_π, and $\rho_\pi{}^*$ can be calculated from eq 13. To set up these equations, a set of spin-unrestricted calculations on CN have been carried out, in which a single electron has been placed on $3a_1$, 1e, and 2e. The calculations have shown that the single spin localizes mainly on C

$$\rho_\sigma(C) = 0.815\rho_\sigma$$
$$\rho_\pi(C) = 0.300\rho_\pi + 0.77\ \rho_\pi{}^* \qquad (13)$$
$$\rho_\pi(N) = 0.700\rho_\pi + 0.224\rho_\pi{}^*$$

with probabilities of 0.815 and 0.776 for $3a_1$ and 2e, respectively, and mainly on N with a probability of 0.700 for 1e. The calculated values of ρ_σ, ρ_π, and $\rho_\pi{}^*$ are included in Table 3, and they confirm our interpretation based on qualitative arguments. Thus, ρ_σ is found to be negative, except for cases with singly occupied d_{z^2} orbitals on M^{III}. ρ_π is positive, in agreement with the spin delocalization mechanism taking place by π-type LMCT (Figure 4a). Finally, $\rho_\pi{}^*$ are negative and indicative of rather strong electron correlation effects, involving the 2e orbital of CN^-. It is interesting that the overall π contributions (sum of ρ_π and $\rho_\pi{}^*$) are in favor of a π-delocalization mechanism. With the set of values ρ_σ, ρ_π, and $\rho_\pi{}^*$, we can calculate the $Cu^{II}-M^{III}$ exchange coupling constant based on the approximate eq 10. In this equation j_σ, j_π, and j_{π^*} are exchange coupling constants for the interaction between the unpaired spin of Cu^{II} and the one of the CN radical with a spin on the $3a_1$, 1e, and 2e orbitals, respectively. Results from spin-unrestricted calculations that yield these metal−radical coupling constants are visualized in Figure 5, along with the spin density plots. Note the accumulation of β spin density on the C-end of the Cu−NC moiety, similar to the MCN fragment. Cu−NC metal radical coupling energies are as expected rather large, with exchange constants following the order $j_\pi > j_\sigma > j_{\pi^*}$. A nice correlation between values J' and J_{BS} is obtained (Figure 6), with the critical points of $^6A_1(Fe)$ and $^5A_1(Mn)$, which now lie exactly on the line (see also Figure 3).

The approximation of the $Cu^{II}-M^{III}$ exchange coupling constant as a weighted sum over the parameters j_σ, j_π, and j_{π^*} with the corresponding spin densities ρ_σ, ρ_π, and $\rho_\pi{}^*$ as weighting factors allows us to decompose the total energy J' into $J'(\sigma)$, $J'(\pi)$, and $J'(\pi^*)$ terms (Table 4). Although the $J'(\sigma)$ and $J'(\pi^*)$ terms are negative (antiferromagnetic), $J'(\pi)$ is ferromagnetic and dominates the sign of the overall coupling energy J'. The comparison between the values of J' for the *trans*-

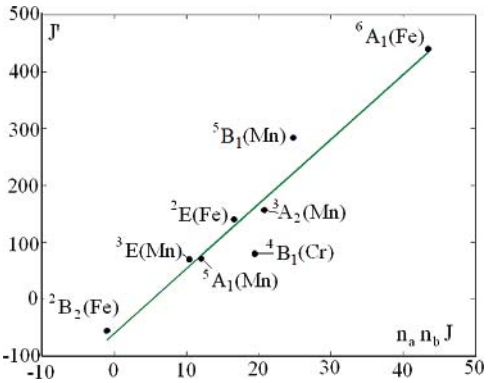

Figure 6. Correlation between J' and $n_a n_b J_{BS}$; $J' = 11.36\ (n_a n_b J_{BS}) - 60.5$.

$[M^{III}(NH_3)_4(CN)_2]^+$ model complex and for $[M(CN)_6]^{3-}$ shows that the $Cu^{II}-M^{III}$ exchange coupling is weakly affected by the nature of the equatorial ligands. The same result was obtained when $J_{BS}(Cu^{II}-NC-Cr^{III})$ was calculated directly [$J_{BS} = 5.2$ cm^{-1}(CN), $J_{BS} = 6.8$ cm^{-1} (NH_3)]. Only for Mn^{III} [$^3E(b_2{}^1e^3)$] and Fe^{III}[$^2E(b_2{}^2e^3)$], and to lesser extent for Fe^{III}[$^6A_1(b_2{}^1e^2b_1{}^1a_1{}^1)$] we obtain lower values of J' when replacing NH_3 by CN^-.

We have confined our spin-density analysis of the exchange coupling to complexes with a linear $Cu^{II}-NC-M^{III}$ bridge and ferromagnetic $Cu^{II}-M^{III}$ coupling. Spin population analysis of the exchange coupling in the case of homo nuclear antiferromagnetically coupled pairs of $s = {}^1/_2$ transition-metal ions have been used to relate the exchange coupling constants from broken-symmetry calculations with the spin density on the magnetic ions in the high-spin (ρ_{HS}) and broken-spin (ρ_{BS}) states[15]

$$J_{BS} \approx -U(\rho_{HS}{}^2 - \rho_{BS}{}^2) \qquad (14)$$

Antiferromagnetic coupling is predicted for $\rho_{HS} > \rho_{BS}$. However, it has been pointed out that in certain cases, such as in end-on azide-bridged Cu_2 pairs, ρ_{HS} can become smaller than ρ_{BS}, and this leads to ferromagnetic coupling. It is interesting to note when focusing on the Cu−CN−Cr pair (Table 5) that $\rho_{HS} < \rho_{BS}$ results for the $Cu^{II}-Cr^{III}$ pair, thus being consistent with eq 14 and ferromagnetic $Cu^{II}-Cr^{III}$ coupling. This also emerges for $Cu^{II}-Mn^{III}$ and $Cu^{II}-Fe^{III}$ pairs (see the Supporting Information). A generalized form of eq 14 has led to an approximate equation for heterodinuclear complexes with spin densities on centers 1 and 2 denoted by ρ_{HS1},ρ_{BS1} and ρ_{HS2},ρ_{BS2}, respectively:[14,56]

$$n_a{\cdot}n_b J_{BS} \propto \Delta = [|\rho_{HS1}{}^2 - \rho_{BS1}{}^2|^{1/2} + |\rho_{HS2}{}^2 - \rho_{BS2}{}^2|^{1/2}]^2 \qquad (15)$$

The $n_a{\cdot}n_b J_{BS}$ versus Δ plot (see the Supporting Information) shows a clear correlation. However, this correlation is less pronounced, compared to that obtained with eq 10 (Figure 6). It follows that explicit consideration of the electronic structure of the bridging cyanide ligand is needed in order to relate the exchange coupling energies with the underlying spin density distributions.

Dependence of the Exchange Coupling on the Orbital Occupancy and Exchange Anisotropy in the Case of Orbitally Degenerate States: The Linear Cu−NC−Fe Exchange Pair. Two different (opposing) forces operate within the $^3T_1$ and $^2T_2$ ground states of low-spin octahedral Mn^{III} and Fe^{III} complexes and tend to lift the orbital degeneracy; Jahn−Teller

TABLE 4: Exchange Coupling (Denoted Hereafter as J' [b]) Deduced from a SPSD-Model Using *trans*-$M(NH_3)_4(CN)_2^{1+}$ and $M(CN)_6^{3-}$ Building Blocks[a]

Cu^{II}-M^{III} pair (M^{III} electronic configuration)	$[Cu(NH_2CH_3)_4-NC-M^{III}CN(NH_3)_4]^{3+}$				$[Cu(NH_2CH_3)_4-NC-M^{III}(CN)_5]^{1-}$			
	J'	$J'(\sigma)$	$J'(\pi)$	$J'(\pi^*)$	J'	$J'(\sigma)$	$J'(\pi)$	$J'(\pi^*)$
$Cu^{II}-NC-Cr^{III}$								
$^4B_1(b_2^1e^2)$	220	−129	430	−81	242	−130	456	−84
$Cu^{II}-NC-Mn^{III}$								
$^3A_2(b_2^2e^2)$	248	−101	422	−73	222	−99	390	−69
^3E $(b_2^1e^3)$	125	−78	246	−42	72	−77	190	−41
$^5A_1(b_2^1e^2b_1^1)$	171	−157	404	−75	173	−143	392	−77
$^5B_1(b_2^1e^2a_1^1)$	374	53	380	−57	386	150	281	−44
$Cu^{II}-NC-Fe^{III}$								
$^2E(b_2^2e^3)$	190	−48	277	−38	98	−42	178	−32
$^2B_2(b_2^1e^4)$	−46	−42	−2	−2	−48	−35	−8	−4
$^6A_1(b_2^1e^2b_1^1a_1^1)$	525	190	456	−51	401	91	228	−32

[a] The decomposition of J' into contributions from $Cu^{II}-\pi(CN)$, $\pi^*(CN)$, and $\sigma(CN)$ metal−radical coupling energies are also given. All energies in cm^{-1}. [b] $J' = c_\sigma \cdot j_\sigma + c_\pi \cdot j_\pi + c_{\pi^*} \cdot j_{\pi^*}$; values of $j_\sigma = 1400$ cm^{-1}, $j_\pi = 2020$ cm^{-1}, and $j_{\pi^*} = 510$ cm^{-1} have been deduced as energies due to $Cu(NH_2CH_3)_4-NC$ metal $Cu^{2+}(d^9)-CN$ radical coupling.

TABLE 5: Atomic (Mulliken) Spin Populations for the CuNCCr Pair in Its High-Spin (HS) and Broken-Spin (BS) State as Well as for the Separate Cu and NCCr Magnetic Building Units

	Cu	N	C	Cr
HS	0.460	0.086	−0.100	3.194
BS	0.468	0.081	−0.095	3.190
Cu	0.455			
NCCr		0.114	−0.127	3.188

coupling, which we neglect in a first approximate,[57] and spin−orbit coupling.

The latter leads to a splitting of the $^3T_1$ and $^2T_2$ states into A_1, T_1, and E,T_2 (accidentally degenerate; for $^3T_1$) and Γ_7 and Γ_8 (for $^2T_2$) in the order of increasing energy with energy separations of the order of the spin−orbit coupling constant. At very low temperature only the states A_1 (for Mn^{III}) and Γ_7 (for Fe^{III}) are thermally populated with effective g-tensor values of zero and (1/3) (2 + 4*k*) (*k*, the covalent reduction factor), respectively. Thus Mn^{III} is nonmagnetic, whereas Γ_7 of Fe^{III} behaves as a $s = {}^1/_2$ Kramers doublet. We focus on the latter ion and consider the $Cu^{II}-NC-Fe^{III}$ exchange pair. The Γ_7 (Fe^{III}) wave function is given by

$$\Psi\left(\Gamma_7, m_s = \frac{1}{2}\right) = \sqrt{\frac{2}{3}}\left|-1, \frac{1}{2}\right\rangle - \sqrt{\frac{1}{3}}\left|0, -\frac{1}{2}\right\rangle$$

$$\Psi\left(\Gamma_7, m_s = -\frac{1}{2}\right) = \sqrt{\frac{2}{3}}\left|1, -\frac{1}{2}\right\rangle - \sqrt{\frac{1}{3}}\left|0, \frac{1}{2}\right\rangle \quad (16)$$

where 0, and ±1 refer to the M_L values of the $L = 1$ angular momentum eigenfunctions and $\pm{}^1/_2$ denote the m_s components of the $s = {}^1/_2$ spin. As can be shown, the ±1 and 0 orbital functions give rise to the real d_{yz}, d_{xz}, and d_{xy} orbitals, respectively. It follows from eq 16 that it is the linear combination of BS-DFT exchange coupling parameters for the Cu−Fe (^2E) and Cu−Fe ($^2B_2$) pairs (Table 2, 16.6 cm^{-1} and −1.0 cm^{-1}, respectively) rather than each single determinant J_{BS}, which yields the exchange interaction for the Cu−Fe (Γ_7) pair. In this case, orbital degeneracy exchange coupling is described by an orbital-dependent exchange operator.[24−26] The application of this formalism to the Cu−NC−Fe (Γ_7) exchange pair (see the Supporting Information) leads to the following exchange operator

$$H_{exc} = -J \cdot \mathbf{S_1}\mathbf{S_2} + D\left[\mathbf{S_z}^2 - \frac{1}{3}S(S+1)\right] \quad (17)$$

written within the direct product of two coupling $s = {}^1/_2$ pseudospins and the following dependence of its eigenvalues on the total spin $S = 0$, 1 and $M_s = 0$, ±1 quantum numbers:

$$E(S) = -\frac{J}{2}\left[S(S+1) - \frac{3}{2}\right] + D\left(M_s^2 - \frac{2}{3}\right) \quad (18)$$

If we neglect the small contribution of the exchange of Cu−Fe ($^2B_2$), the isotropic (*J*) and the anisotropic (*D*) parameters are given by the following expression in terms of the $J(^2E)$ energy (16.6 cm^{-1}, Table 2):

$$J = \frac{2}{9}J(^2E) \quad (19)$$

$$D = -\frac{1}{3}J(^2E)$$

As immediately follows from eq 24, *J* is reduced by a factor of about five ($J = 3.6$ cm^{-1}), compared to its nominal $J(^2E)$ BS-DFT value. In addition, a negative and about twice larger than *J* anisotropic contribution *D* (−5.4 cm^{-1}) results, which leads to stabilization the $M_s = \pm 1$ pair of states against the $M_s = 0$ one. The effect of anisotropy gets even larger when going to extended linear complexes $Cu^{II}-Fe^{III}-Cu^{II}$ and further to $Mn^{II}-Fe^{III}-Mn^{II}$ (with an $s = {}^5/_2$ high-spin state on Mn^{II}).[58] However, a vibronic reduction of this anisotropy in the case of a dynamic Jahn−Teller coupling of the $^2T_{2g}$ ground state of $[Fe(CN)_6]^{3-}$ with the trigonal distortion mode (Γ_2) is expected to take place.[57]

The strong reduction of the isotropic exchange constant and the appearance of large anisotropic contributions allows us to conclude that reported DFT values of the exchange coupling constants for a series of cyanide bridged exchange pairs[14] [more explicitly $Mn^{III}V^{II}$ ($t_{2g}^4-t_{2g}^3$), $Cr^{III}Mo^{II}$($t_{2g}^3-t_{2g}^4$), $V^{III}V^{II}$-($t_{2g}^2-t_{2g}^3$), $Mn^{III}Cr^{II}$ ($t_{2g}^4-t_{2g}^3e_g^1$), $Cr^{III}V^{IV}$($t_{2g}^3-t_{2g}^1$), $Cr^{III}V^{III}$-($t_{2g}^3-t_{2g}^2$), $Mn^{III}V^{III}$($t_{2g}^4-t_{2g}^2$), $V^{III}Ni^{II}$ ($t_{2g}^2-t_{2g}^6e_g^2$), $Ti^{III}Cr^{III}$-($t_{2g}^1-t_{2g}^3$), and $Ti^{III}V^{II}$($t_{2g}^1-t_{2g}^3$)] are not correct and should be regarded with great care. However, when applied to high T_c magnets with cubic perowskite structure[14] anisotropy may cancel partly or completely. Under such conditions, ferrimagnetic couplings are not expected to be affected largely by anisotropy. However, in polynuclear magnetic clusters with symmetry lower than cubic, anisotropy may play an important role. We have shown that BS-DFT values of the exchange coupling parameters deduced from single determinants could be very useful when calculating exchange coupling energies between spin−orbit split multiplets, such as the just illustrated $Cu^{II}-NC-Fe^{III}$ model

example. This is of great importance for a more systematic search in molecular magnetism.

Conclusions

(1) Magnetic coupling across the CN bridge is governed by pathways that involve $\pi[t_{2g}(d_{xz,yz})$, 1e(CN)], $\pi^*[t_{2g}(d_{xz,yz})$, 2e(CN)], as well as $\sigma[e_g(d_{z^2})$, $3a_1$(CN)] (M−CN) orbitals. The σ interactions are usually neglected.

(2) If d_{z^2} is empty, then CN → M transfer leads to β spin density contributions of C and N, which weakens the magnitude of the Cu−M exchange coupling constants dominated by α-spin densities.

(3) If d_{z^2} is singly occupied, then both σ- and π-transferred spin densities are of α type, and this enhances the ferromagnetic exchange interactions. Because, for the strong CN ligand, single occupancy of d_{z^2} takes place in high-spin, metastable excited states, this opens new aspects of interest for molecular photomagnetism.

(4) A new concept for the calculation of magnetic exchange coupling constants, based on spin densities of the magnetic building blocks of a dinuclear transition metal complex, is presented and applied to Cu^{II}−NC−M^{III} pairs at a phenomenological level. In a first step, the spin density is calculated on the CN bridge of the M^{III}−CN complex. In a second step, the coupling of a single $CN^{\bullet}$ radical with the Cu^{II} complex is computed, considering various orbital configuration of the unpaired electron. Finally, the information from the spin-density calculations of the first step is used to properly reduce the Cu−CN metal radical exchange constants, and this yields the Cu−NC−M dimer exchange coupling constant. Values of *J*, deduced from this model, are systematically larger than those from broken-symmetry calculations because DFT overestimates metal−ligand covalency. However, there is a nice linear correlation between the two sets of *J* values. The new approach allows us to analyze the exchange coupling across the CN bridge in terms of the pathways, which involve the σ, π, and π^* orbitals of CN. The application to the Cu^{II}−CN−M^{III} pairs shows that the ferromagnetic exchange constant is dominated by spin delocalization over the fully occupied CN π orbital; both spin polarization and delocalization which involve the occupied σ and the empty π^* molecular orbitals are nonnegligible, and the latter yield negative (antiferromagnetic) contributions to J'.

(5) The inclusion of orbital dependence of the exchange coupling leads to a large exchange coupling anisotropy in linear Cu^{II}−NC−Fe^{III} pairs, and this is found to further increase in pairs Cu^{II}−Fe^{III}−Cu^{II} and Mn^{II}−Fe^{III}−Mn^{II} (with $s = {}^5/_2$ spin on Mn).

(6) One needs to be cautious when calculating exchange coupling constants with the BS-DFT approach in the case of transition metals with T_1 and T_2 orbitally degenerate states. Mixing between orbital configurations via the spin−orbit coupling operator can strongly modify the DFT predicted values of isotropic exchange coupling constants.

Acknowledgment. Financial support by the Deutsche Forschungsgemeinschaft (SPP 1137 "Molecular Magnetism") and the Swiss Bundesamt für Bildung und Wissenschaft are gratefully acknowledged.

Supporting Information Available: Data on the effect of the functional, data related to Figure 2, and a theoretical analysis of the exchange coupling. This material is available free of charge via the Internet at http://pubs.acs.org.

References and Notes

(1) Kahn, O. *Molecular Magnetism*; Wiley&Sons Inc.: New York, 1993.
(2) Miller, J. S.; Drillon, M. In *Magnetism: Molecules to Materials*; Wiley-VCH: Weinheim, Germany, 2001−2004; Vol. 1−4.
(3) Ferlay, S.; Mallah, T.; Ouahes, R.; Veillet, P.; Verdaguer, M. *Nature (London)* **1995**, *378*, 701.
(4) Weihe, H.; Güdel, H. U. *Comments Inorg. Chem.* **2000**, *22*, 75.
(5) Mironov, V. S.; Chibotaru, L. F.; Ceulemans, A. *J. Am. Chem. Soc.* **2003**, *125*, 9750.
(6) Verdaguer, M.; Bleuzen, A.; Train, C.; Garde, R.; deBiani, F. F.; Desplanches, C. *Philos. Trans. R. Soc. London, Ser. A* **1999**, *357*, 2959.
(7) Verdaguer, M.; Bleuzen, A.; Marvaud, V.; Vaissermann, J.; Seuleiman, M.; Desplanches, C.; Scuiller, A.; Train, C.; Garde, R.; Gelly, G.; Lomenech, C.; Rosenman, I.; Veillet, P.; Cartier, C.; Villain, F. *Coord. Chem. Rev.* **1999**, *192*.
(8) Kahn, O.; Briat, B. *J. Chem. Soc., Faraday Trans. 1* **1976**, *72*, 268.
(9) Kahn, O.; Briat, B. *J. Chem. Soc., Faraday Trans. 1* **1976**, *72*, 1441.
(10) Eyert, V.; Siberchicot, B.; Verdaguer, M. *Phys. Rev. B* **1997**, *56*, 8959.
(11) Harrison, N. M.; Searle, B. G.; Seddon, E. A. *Chem. Phys. Lett.* **1997**, *266*, 507.
(12) Nishino, M.; Takeda, S.; Mori, W.; Nakamura, A.; Yamaguchi, K. *Synth. Met.* **1997**, *85*, 1763.
(13) Nishino, M.; Yoshioka, Y.; Yamaguchi, K. *Chem. Phys. Lett.* **1998**, *297*, 51.
(14) Ruiz, E.; Rodriguez-Fortea, A.; Alvarez, S.; Verdaguer, M. *Chem.—Eur. J.* **2005**, *11*, 2135.
(15) Blanchet-Boiteux, C.; Mouesca, J.-M. *J. Am. Chem. Soc.* **2000**, *122*, 861.
(16) Cano, J.; Ruiz, E.; Alvarez, S.; Verdaguer, M. *Comments Inorg. Chem.* **1998**, *20*, 27.
(17) Bersuker, I. B. *J. Comput. Chem.* **1997**, *18*, 260.
(18) Atanasov, M.; Daul, C. A. *Chimia* **2005**, *59*, 504.
(19) Atanasov, M.; Daul, C. A.; Rauzy, C. *Chem. Phys. Lett.* **2003**, *367*, 737.
(20) Anthon, C.; Benix, J.; Schaffer, C. E. *Inorg. Chem.* **2003**, *42*, 4088.
(21) Atanasov, M.; Daul, C. A.; Rauzy, C. *Struct. Bonding (Berlin)* **2004**, *106*, 97.
(22) Anthon, C.; Bendix, J.; Schaffer, C. E. *Inorg. Chem.* **2003**, *43*, 7882.
(23) Atanasov, M.; Daul, C.; Güdel, H. U.; Wesolowski, T. A.; Zbiri, M. *Inorg. Chem.* **2005**, *44*, 2954.
(24) Palii, A. V.; Tsukerblat, B. S.; Verdaguer, M. *J. Chem. Phys.* **2002**, *117*, 7896.
(25) Tsukerblat, B. S.; Palii, A. V.; Ostrovsky, S. M.; Kunitsky, S. V.; Klokishner, S. I.; Dunbar, K. R. *J. Chem. Theory Comput.* **2005**, *1*, 668.
(26) Palii, A. V.; Ostrovsky, S. M.; Klokishner, S. I.; Tsukerblat, B.; Dunbar, K. R. *ChemPhysChem* **2006**, *7*, 871.
(27) Atanasov, M.; Comba, P.; Lampeka, Y. D.; Linti, G.; Malcherek, T.; Miletich, R.; Prikhod'ko, A. I.; Pritzkow, H. *Chem.—Eur. J.* **2006**, *12*, 737.
(28) Following Cano et al. (ref 16) and the discussion therein, we use the notion of spin density in the sense of spin population as calculated from a spin-unrestricted calculation using Mulliken population analysis.
(29) Noodleman, L.; Norman, J. G., Jr. *J. Chem. Phys.* **1979**, *70*, 4903.
(30) Noodleman, L. *J. Chem. Phys.* **1981**, *74*, 5737.
(31) Noodleman, L.; Davidson, E. R. *Chem. Phys.* **1986**, *109*, 131.
(32) Ruiz, E.; Alvarez, S.; Cano, J. *J. Chem. Phys.* **2005**, *123*, 164110.
(33) Ruiz, E.; Cano, J.; Alvarez, S.; Polo, V. *J. Chem. Phys.* **2006**, *124*, 107102.
(34) Adamo, C.; Barone, V.; Bencini, A.; Broer, R.; Filatov, M.; Harrison, N. M.; Illas, F.; Malrieu, J. P.; Moreira, I. de P. R. *J. Chem. Phys.* **2006**, *124*, 107101.
(35) McConnel, H. M. *J. Chem. Phys.* **1963**, *39*, 1910.
(36) Deumal, M.; Novoa, J. J.; Bearpark, M. J.; Celani, P.; Olivucci, M.; Robb, M. A. *J. Phys. Chem. A* **1998**, *102*, 8404.
(37) Novoa, J. J.; Deumal, M. *Struct. Bonding (Berlin)* **2001**, *100*, 33.
(38) Bertrand, P. *Inorg. Chem.* **1993**, *32*, 741.
(39) Clark, A. E.; Davidson, E. R. *J. Chem. Phys.* **2001**, *115*, 7382.
(40) O'Brien, T. A.; Davidson, E. R. *Int. J. Quantum Chem.* **2003**, *92*, 294.
(41) Bérces, A.; Bo, C.; Boerrigter, P. M.; Cavallo, L.; Chong, D. P.; Deng, L.; Dickson, R. M.; Ellis, D. E.; Fan, L.; Fischer, T. H.; Fonseca Guerra, C.; van Gisbergen, S. J. A.; Groeneveld, J. A.; Gritsenko, O. V.; Grüning, M.; Harris, F. E.; van den Hoek, P.; Jacobsen, H.; van Kessel, G.; Kootstra, F.; van Lenthe, E.; McCormack, D. A.; Osinga, V. P.; Patchkovskii, S.; Philipsen, P. H. T.; Post, D.; Pye, C. C.; Ravenek, W.; Ros, P.; Schipper, P. R. T.; Schreckenbach, G.; Snijders, J. G.; Sola, M.; Swart, M.; Swerhone, D.; te Velde, G.; Vernooijs, P.; Versluis, L.; Visser, O.; van Wezenbeek, E.; Wiesenekker, G.; Wolff, S. K.; Woo, T. K.;

Baerends, E. J.; Autschbach, J.; Ziegler, T. *ADF2004.01 SCM*; Theoretical Chemistry: Vrije Universiteit: Amsterdam, The Netherlands, 2004.
(42) Baerends, E. J.; Ellis, D. E.; Ros, P. *Chem. Phys. Lett.* **1993**, *2*, 42.
(43) Boerrigter, P. M.; te Velde, G.; Baerends, E. J. *Int. J. Quantum Chem.* **1988**, *33*, 87.
(44) te Velde, G.; Baerends, E. *J. Comput. Phys.* **1992**, *99*, 84.
(45) te Velde, G.; Bickelhaupt, F. M.; Baerends, E. J.; Fonseca Guerra, C.; van Gisbergen, S. J. A.; Snijders, J. G.; Ziegler, T. *J. Comput. Chem.* **2001**, *22*, 931.
(46) van Lenthe, E.; Baerends, E. J.; Snijders, J. G. *J. Chem. Phys.* **1993**, *99*, 4597.
(47) Vosko, S. H.; Wilk, L.; Nusair, M. *Can. J. Phys.* **1980**, *58*, 1200.
(48) Perdew, J. P.; Wang, Y. *Phys. Rev. B* **1986**, *33*, 8800.
(49) Perdew, J. P.; Chevary, J. A.; Vosko, S. H.; Jackson, K. A.; Pederson, M. R.; Singh, D. J.; Fiolhais, C. *Phys. Rev. B* **1992**, *46*, 6671.
(50) Neese, F. *ORCA*, version 2.4, an ab initio, density functional, and semiempirical program package; Max-Planck-Institut für Bioanorganische Chemie: Mülheim an der Ruhr, Germany, 2005. http://www.thch.uni-bonn.de/tc/orca.
(51) Klamt, A.; Schürmann, G. *J. Chem. Soc., Perkin Trans. 2* **1993**, 799.
(52) Pye, C. C.; Ziegler, T. *Theor. Chem. Acc.* **1999**, *101*, 396.
(53) Figgis, B. N.; Forsyth, J. B.; Reynolds, P. A. *Inorg. Chem.* **1987**, *26*, 101.
(54) Figgis, B. N.; Forsyth, J. B.; Mason, R.; Reynolds, P. A. *Chem. Phys. Lett.* **1985**, *115*, 454.
(55) Köhler, F. H.; Lescouëzec, R. *Angew. Chem., Int. Ed.* **2004**, *43*, 2571.
(56) The equation $n_a \cdot n_b J_{BS} \propto \Delta = [(\rho_{HS1}^2 - \rho_{BS1}^2)^{1/2} + (\rho_{HS2}^2 - \rho_{BS2}^2)^{1/2}]^2$ derived in ref 14 needs to be modified to account for situations where $\rho_{HS1} < \rho_{LS1}$ and $\rho_{HS2} < \rho_{LS2}$.
(57) Atanasov, M.; Comba, P. *J. Mol. Struct.*, submitted for publication.
(58) Atanasov, M.; Busche, C.; Comba, P.; Rajaraman, G.; Wadepohl, H., to be submitted for publication.